Petroleum Science 23 (2026) 818–835

Contents lists available at ScienceDirect

Petroleum Science

journal homepage: www.keaipublishing.com/en/journals/petroleum-science

Original Paper

Performance evaluation of multilateral horizontal wells on flow characteristics and recovery efficiency based on coupled model

Chun-Xue Cui [a,b], Xiao-Long Chai [c,d,e,*], Yue-Wu Liu [a,b], Zhi-Jun Zhou [f], Guo-Qing Zhang [f], Leng Tian [c,d,e]

[a] Institute of Mechanics, Chinese Academy of Sciences, Beijing, 100190, China
[b] University of Chinese Academy of Sciences, Beijing, 100049, China
[c] State Key Laboratory of Petroleum Resources and Engineering, China University of Petroleum (Beijing), Beijing, 102249, China
[d] Institute of Petroleum Engineering, China University of Petroleum (Beijing), Beijing, 102249, China
[e] Research Center for Natural Gas Geology and Engineering, China University of Petroleum (Beijing), Beijing, 102249, China
[f] Key Laboratory of Enhanced Oil Recovery, Northeast Petroleum University, Daqing, 163000, Heilongjiang, China

ARTICLE INFO

Article history:
Received 9 March 2025
Received in revised form
24 June 2025
Accepted 24 October 2025
Available online 30 October 2025

Edited by Meng-Jiao Zhou

Keywords:
Coupled model
Multilateral horizontal wells
Water breakthrough
Enhance oil recovery
Bottom water reservoir

ABSTRACT

The multi-branch horizontal wells can improve the reservoir dynamic flow profile, restrain water coning, enhance production and recovery efficiency due to large drainage area and low cost, and it is significant importance for academic research and industrial applications. However, the effects of branches interference and wellbore variable mass flow on transient dynamics of water breakthrough, production characteristics and recovery efficiency have long been ignored. To dynamically simulate and evaluate the fluid flow behavior of multilateral horizontal wells, first, the branches interference and coupled relationship between reservoir fluid seepage and wellbore variable mass flow has been investigated in this paper, a coupled model for predicting multilateral horizontal wells dynamic production and water breakthrough time is proposed with arbitrary three-dimensional spatial distribution. Subsequently, the model is validated by comparing the production and breakthrough time between actual production data and simulated software. Last, the performance characteristics including inflow dynamics, production, wellbore pressure drop and water breakthrough dynamic distribution are analyzed. The results indicate that the unstable flow time is shorten and it is about 0.6 h, and the wellbore inflow profile represents a characteristic of "low in the middle and high at both ends" on account of branches interference. The pressure drop of wellbore is mainly affected by friction, and other pressure drop types are acceleration pressure drop, convergence pressure drop and mixed pressure drop in order of influence, respectively. The breakthrough time is prior at junction of main wellbore and branch wellbores, then the bottom water spreads to the middle position of main wellbore and trailing position of each branch wellbore. The branch length has a critical impact on breakthrough time, and the branch numbers also affect it as well as the branch angle. The proposed theoretical model can be used to calculate and predict the production, breakthrough time and recovery efficiency of multilateral horizontal wells, and it supplies strong technical support for further development and enhance oil recovery of bottom water reservoir and actual oil field production.

1. Introduction

Multi-branch horizontal wells have become widely application in both domestic and international oil fields, particularly in offshore oil fields (Bazitov et al., 2015; Fan et al., 2006; Wang et al., 2025a, b; Yue et al., 2015), which improves the reservoir dynamic flow profile, slows down the bottom water coning rate, delays the water breakthrough time, and increases the recovery degree

* Corresponding author.
E-mail address: chaixiaolong1991@126.com (X.-L. Chai).
Peer review under the responsibility of China University of Petroleum (Beijing).

https://doi.org/10.1016/j.petsci.2025.10.025

(Wang et al., 2015; Filho et al., 2015; Zhou et al., 2016; Zhang et al., 2023). The fundamental assurances for attaining favorable economic outcomes when multilateral horizontal wells are put into production are delaying bottom water coning and precisely forecasting production (Song et al., 2019; Shi et al., 2023, 2024). Since Muskat and Wyckoff (1935) introduced the concept of water coning into the petroleum engineering field, numerous researchers have been thoroughly examined analytical solutions and empirical correlations to predict the productivity (Bruining et al., 1991; McCarthy, 1994; Permadi and Jayadi, 2010; Luo et al., 2008, 2017; Bahadori and Nouri, 2012) and water breakthrough dynamics for vertical (Tabatabaei et al., 2012; Bournazel and Jeanson, 1971; Cai, et al., 2024, 2025; Ozkan and Raghavan, 1989) or horizontal wells (Ozkan and Raghavan, 1990; Permadi and Jayadi, 2010; Permadi et al., 1995). Zhou et al. (2023) derived a transient productivity prediction model of perforated multilateral horizontal wells by considering the mutual interference between branches and perforations, but not considered the wellbore pressure drop. Yue et al. (2021) concentrated on the pressure drop in the wellbore, developed the multilateral horizontal well productivity model and examined the productivity-sensitive factors, however, they did not take production time into account. Wang et al. (2015) investigated the remaining oil distribution rules, formation mechanisms, and enhance oil recovery (EOR) methods through physical experiments on acrylic models resembling the geological features of reservoirs, revealed the significant effects of fracture cave morphological configuration and connectivity on remaining oil distribution, provided new insights and guidance for EOR design optimization catering to the unique features of fractured vuggy reservoirs. Gang et al. (2024) established a new horizontal well productivity prediction model by coupling key geological and engineering parameters, calculated the similarity coefficient and realized quantitative prediction of single well productivity. Yue et al. (2020) proposed a new coupling model for estimating the water breakthrough time of complex structured multilateral horizontal wells, and the coupling model shows an excellent agreement with the results from the actual scenarios. However, they did not take variable-mass flow pressure drop into account. On this basis, many studies have proposed that the branch angle is an important factor causing interference between branches (Tong et al., 2024; Zhang and Gu, 2024; Qiu et al., 2023; Yi and Tang, 2023). For multilateral horizontal wells, the interaction among laterals can also influence productivity (Fuad and Qasem, 2024; Lux et al., 2016). The parameters related to the shape of multilateral horizontal wells, such as branch length and branch angles, can obviously affect the productivity and water breakthrough dynamics (Wang et al., 2017; Yu et al., 2019). However, due to the complex structure of multilateral horizontal wells, there aren't many productivity studies that take into account the effect of wellbore variable mass flow pressure drop and the dynamic flow performances in bottom water reservoir (Zhai et al., 2022). Specifically, the influence of branch parameters on the water coning and cresting dynamics is not clearly understood yet. Therefore, in order to manage the challenges in the bottom water reservoir development process, effectively guide on-site production operations and forecast productivity, bottom water breakthrough time and location distribution along the wellbores, a trustworthy model is required. In this paper, combining the theories of flow in porous media, engineering fluid mechanics and reservoir engineering, a coupled model of reservoir percolation and wellbore variable mass flow that takes into consideration wellbore mutual interference is established by using the mathematical and physical approach. The model can describe the various components that make up wellbore pressure drop and fluid flow characteristics, explain the mutual interference between wellbores and the water breakthrough dynamics, including water breakthrough time and location. Compared to previous studies, the proposed model took multiple factors into account, including the wellbore pressure drop composition, the coupling relationship between reservoir and wellbore flow and the impact of production time, which brings the results closer to the actual production of oil fields. The coupling flow production and water breakthrough model of multilateral horizontal well from previous works were obtained (Table 1). The study is important for improving the recovery efficiency, determining a reasonable working system, delaying water breakthrough, optimizing the layout mode and spatial structure of multilateral horizontal wells in the bottom water reservoirs.

2. Model construction

2.1. Physical model

The fishbone drilling technique in a bottom water reservoir is distinguished by micro-holes branching from the primary horizontal well, with sidetracks I, II, III, and IV along the main wellbore (Fig. 1). The reservoir's top surface is a closed boundary, while its bottom surface is a constant pressure boundary. The reservoir thickness is h, the reservoir anisotropic permeability is $k_x = k_y = k_h$, $k_z = k_v$, the distance between the wellbore and the oil-water interface is z_w, the length of each branch is equal. Fluid flows simultaneously to the main wellbore production section and the branch wellbore production section. Ignoring the effects of capillary forces and gravity, the reservoir fluid is single-phase, slightly compressible and flow follows Darcy's law. The multilateral horizontal well can be arranged in any way, with varying numbers, shapes, and configurations.

2.2. Mathematical model

2.2.1. Productivity coupling model of multilateral horizontal wells

Model I is the multilateral horizontal wells productivity coupling model in bottom reservoirs, which composed of reservoir percolation model and wellbore variable mass flow pressure drop model. The development and resolution of model are the foundation for dynamic prediction, parameter sensitivity analysis, and water breakthrough dynamic analysis of multilateral horizontal wells.

In bottom water reservoir, the slightly compressible fluid flows to the multilateral horizontal well production section satisfies Eq. (1):

$$k_h\frac{\partial^2 p}{\partial x^2}+k_h\frac{\partial^2 p}{\partial y^2}+k_v\frac{\partial^2 p}{\partial z^2}=\phi\mu C_t\frac{\partial p}{\partial t} \tag{1}$$

The initial and boundary conditions are as Eq. (2):

$$\begin{cases} p(x,y,z)|_{t=0}=p_i \\ \left.\dfrac{\partial p}{\partial z}\right|_{z=0}=p_e, \left.\dfrac{\partial p}{\partial z}\right|_{z=h}=0, \lim\limits_{|x|\to\infty}p(x,y,z)=p_i, \lim\limits_{|y|\to\infty}p(x,y,z)=p_i \\ p(x,y,z)|_{(x-x_w)^2+(y-y_w)^2+(z-z_w)^2=r_w^2}=p_{wf}(i)\ (1\le i\le M) \end{cases} \tag{2}$$

In order to facilitate the discussion of multilateral horizontal well pressure distribution, selecting the half length of the main

Table 1
Summary of coupling dynamics model for multilateral horizontal well.

Sources	Models	Methods	Considerations
Luo et al. (2008)	Horizontal wells 3D water cresting model	Experimental methods	Wellbore 3D structure; reservoir and fluids properties
Bahadori and Nouri (2012)	Horizontal wells bottom water coning model	Haugen et al. (1988) analytical method	Formations anisotropic and homogeneous
Tabatabaei et al. (2012)	Vertical wells models of water coning	Analytical solution	Wellbores' length; wellbore radius
Ozkan and Raghavan (1989, 1990)	Horizontal wells water drive model	Mathematical methods	Spacing distance of wellbores; wellbore vertical location
Permadi et al. (1995); Permadi and Jayadi (2010)	Water cresting model of horizontal wells	Analytical method	Reservoir anisotropic; wellbores' length
Zhou et al. (2023)	Transient productivity model of herringbone wells	Analytical method	Mutual interference of branches and perforations; reservoir anisotropic
Yue et al. (2021)	Fishbone multilateral wells production model in the bottom water reservoir	Semi-analytic method	Fishbone structure; wellbores' length; spacing distance of wellbores; wellbore radius; preformation parameters
Yue et al. (2019)	Water breakthrough coupling model for multilateral horizontal well	Semi-analytic method	Wellbore 3D structure; wellbore vertical location; reservoir and fluids properties
Wang et al. (2025b)	Multilateral branch wells oil recovery model	Physical experiments	Remaining oil distribution rules; formation mechanisms
Gang et al. (2024)	Multilateral horizontal well productivity prediction model	Semi-analytic method	Formation pressure; fracturing fluid volume; net pay thickness; permeability
Yue et al. (2020)	Multilateral horizontal wells transient flow model	Analytical method	Mutual interference of branches; production time; reservoir and fluids properties

wellbore as the characteristic length, the dimensionless variable (Ouyang and Aziz, 2001) is expressed as Eq. (3):

$$x_D = \frac{x}{L/2}, y_D = \frac{y}{L/2}, z_D = \frac{z}{L/2}\sqrt{\frac{k_h}{k_v}}, x_{wD} = \frac{x_w}{L/2}, y_{wD} = \frac{y_w}{L/2}, z_{wD} = \frac{z_w}{L/2}\sqrt{\frac{k_h}{k_v}},$$
$$h_D = \frac{h}{L/2}\sqrt{\frac{k_h}{k_v}}, t_D = \frac{3.6k_h}{\varphi C_t \mu (L/2)^2}t, p_D = \frac{hk_h}{1.842\times 10^{-3} q\mu}[p_i - p(x,y,z,t)] \quad (3)$$

where, (x, y, z) is source point; (x_w, y_w, z_w) is field point; (x_D, y_D, z_D) is dimensionless field point; L is the main wellbore length, m; k_h, k_v are the horizontal and vertical permeability of the reservoir, respectively, mD; L_b is the branch wellbore length, m; h is the reservoir thickness, m; ϕ is porosity; C_t is the comprehensive compression coefficient, MPa^{-1}; t is the flow time, h; μ is the oil viscosity, mPa·s; q is the oil production, m^3/d; p is the reservoir pressure, MPa; p_i is the reservoir initial pressure, MPa; p_{wf} is the wellbore pressure, MPa; p_D is the dimensionless reservoir pressure, MPa.

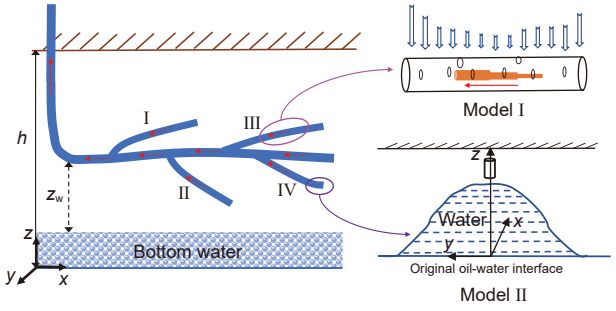

Fig. 1. Schematic diagram of multilateral horizontal well in bottom water reservoir.

(1) Reservoir percolation model

Based on the point source function and microelement theory, the multilateral horizontal well production section is regarded as a

line source that is made up of an infinite number of continuous point sources. According to the study of the continuous point source solution in the top closed-bottom constant pressure reservoir, the pressure drop resulting from the continuous point source $O(x, y, z)$ at any point $M(x_w, y_w, z_w)$ in the Laplace transform domain can be represented as Eq. (4)

$$\overline{\Delta p}(x_{wD}, y_{wD}, z_{wD}, s) = \frac{1.842\times10^{-3}\mu}{L\sqrt{k_v k_h}}\overline{q}(s)\frac{2}{h_D}\left\{\sum_{n=1}^{+\infty}K_0\left[\sqrt{3.6}\,R_{xy,D}\sqrt{s+\frac{(2n-1)^2\pi^2}{3.6\times4h_D^2}}\right]\sin\frac{(2n-1)\pi z_D}{2h_D}\sin\frac{(2n-1)\pi z_{wD}}{2h_D}\right\} \tag{4}$$

where, $R_{xy,D}$ is the dimensionless horizontal distance between the source point $O(x, y, z)$ and the field point $M(x_w, y_w, z_w)$, $R_{xy,D} = \sqrt{(x_{wD}-x_D)^2+(y_{wD}-y_D)^2}$; K_0 is the second class modified Bessel function; n is positive integer; s is the Laplace variable corresponding to t.

Assuming the multilateral horizontal well has N branches, the main wellbore length is L and is divided into M microsegments, the branch wellbore length is L_b and is divided into T microsegments. By integrating the point source solution along the wellbore direction, the pressure drop produced at any point in the reservoir can be determined using the superposition principle. When the multilateral horizontal well main wellbore and branch wellbores are produced simultaneously, considering the interference between the wellbores, the entire production section pressure drop distribution in the bottom water reservoir can be obtained by Eq. (5):

$$\begin{aligned}\Delta\overline{p}(x_{wD}, y_{wD}, z_{wD}, s) &= \Delta\overline{p}_b(x_{wD}, y_{wD}, z_{wD}, s) + \Delta\overline{p}_m(x_{wD}, y_{wD}, z_{wD}, s)\\ &= \frac{1.842\times10^{-3}\mu q}{hk_h}\sum_{j=1}^{N}\sum_{k=1}^{T}2\int_0^{\Delta L_b}\frac{\overline{q}_{br}(j,k)L}{q}\left\{\sum_{n=1}^{+\infty}K_0\left[\sqrt{3.6}\,R_{xy,D}\sqrt{s+\frac{(2n-1)^2\pi^2}{3.6\times4h_D^2}}\right]\sin\frac{(2n-1)\pi z_{jkD}}{2h_D}\sin\frac{(2n-1)\pi z_{wD}}{2h_D}\right\}\frac{dx_{jk}}{2\frac{L}{2}}\\ &+\frac{1.842\times10^{-3}\mu q}{k_h h}\sum_{i=1}^{M}\left\{2\int_0^{\Delta L_m}\frac{\overline{q}_{mr}(i)L}{q}\sum_{n=1}^{+\infty}K_0\left[\sqrt{3.6}\,R_{xy,D}\sqrt{s+\frac{(2n-1)^2\pi^2}{3.6\times4h_D^2}}\right]\sin\frac{(2n-1)\pi z_{miD}}{2h_D}\sin\frac{(2n-1)\pi z_{wD}}{2h_D}\right\}\frac{dx_{mi}}{2\frac{L}{2}}\end{aligned} \tag{5}$$

where, Δp_b is the branch wellbore pressure drop, MPa; Δp_m is the main wellbore pressure drop, MPa; $q_{br}(j, k)$ is the inflow rate of k-th microsegment on the j-th branch, $m^3/(d\cdot m)$; $q_{mr}(i)$ is the inflow rate of main wellbore i-th microsegment, $m^3/(d\cdot m)$; ΔL_b is the microsegment length of branch wellbore, m; ΔL_m is the microsegment length of main wellbore, m; (x_{jk}, y_{jk}, z_{jk}) is the any point of k-th microsegment on the j-th branch; (x_{mi}, y_{mi}, z_{mi}) is the any point of main wellbore i-th microsegment.

The Laplace inverse transform can be used to obtain the expression for the pressure distribution in the time domain, as Eq. (6):

$$\begin{aligned}&\Delta p(x_w, y_w, z_w, t) =\\ &\frac{1.842\times10^{-3}\mu}{hk_hL}\sum_{j=1}^{N}\sum_{k=1}^{T}\int_0^{\Delta L_b}2q_{br}(j,k)\left\{\sum_{n=1}^{+\infty}K_0\left[R_{xy}\frac{(2n-1)\pi}{2h}\right]\sin\frac{(2n-1)\pi z_{jk}}{2h}\sin\frac{(2n-1)\pi z_w}{2h}\right\}dx_{jk}\\ &+\frac{1.842\times10^{-3}\mu}{hk_hL}\sum_{i=1}^{M}\int_0^{\Delta L_m}2q_{mr}(i)\left\{\sum_{n=1}^{+\infty}K_0\left[R_{xy}\frac{(2n-1)\pi}{2h}\right]\sin\frac{(2n-1)\pi z_{mi}}{2h}\sin\frac{(2n-1)\pi z_w}{2h}\right\}dx_{mi}\end{aligned} \tag{6}$$

According to the pressure drop variation rules during variable production, the pressure drop produced at different Δt moments can be expressed as Eq. (7):

$$\begin{aligned}\Delta p(x_w,y_w,z_w,n\Delta t)&=\Delta L_m\sum_{i=1}^{M}q_{mr}(i,n\Delta t)F_i(x_w,y_w,z_w,\Delta t)+\\&\Delta L_m\sum_{i=1}^{M}\sum_{s=1}^{n-1}q_{mr}(i,s\Delta t)\{F_i[x_w,y_w,z_w,(n-s+1)\Delta t]-F_i[x_w,y_w,z_w,(n-s)\Delta t]\}+\\&\Delta L_{bj}\sum_{j=1}^{N}\sum_{k=1}^{T}q_{br}(j,k,n\Delta t)F_{j,k}(x_w,y_w,z_w,\Delta t)+\\&\Delta L_{bj}\sum_{j=1}^{N}\sum_{k=1}^{T}\sum_{s=1}^{n-1}q_{br}(j,k,s\Delta t)\left\{F_{j,k}[x_w,y_w,z_w,(n-s+1)\Delta t]-F_{j,k}[x_w,y_w,z_w,(n-s)\Delta t]\right\}\end{aligned}\tag{7}$$

where, $F_i\,(x_w,y_w,z_w,\Delta t)$ is a function that represents the sum of all terms except for production $\int_0^{\Delta L_m}q_{mr}(\Delta t)$, $\int_0^{\Delta L_{bj}}q_{br}(\Delta t)$ of the main wellbore, MPa·d/m^3; $F_{j,k}\,(x_w,y_w,z_w,\Delta t)$ is a function that represents the sum of all terms except for production $\int_0^{\Delta L_m}q_{mr}(\Delta t)$, $\int_0^{\Delta L_{bj}}q_{br}(\Delta t)$ of the branch wellbore, MPa·d/m^3.

(2) Variable-mass flow pressure drop model

Assuming neither fluid inflow at the wellbore's toe nor heat transfer occurs between the fluid and the wellbore, the conservation of momentum for the production section's i-th infinitesimal segment is represented as Eq. (8):

$$\begin{aligned}\Delta(mV)&=\rho\frac{\pi D_m^2}{4}\left[V_m^2(i)-V_m^2(i+\Delta L_m)\right]\\&=p_{wm}(i+\Delta L_m)\frac{\pi D_m^2}{4}-p_{wm}(i)\frac{\pi D_m^2}{4}-[\tau_{w1}(i)(1-\phi)\\&\quad+\tau_{w2}(i)\phi\pi D_m\Delta L_m]-\rho g\sin\theta\Delta L_m\frac{\pi D_m^2}{4}\end{aligned}\tag{8}$$

where, $V_{mr}(i)$ is the radial flow velocity into the i-th microelement, m/s; $V_m(i)$ is the average flow velocity of the i-th microsegment, m/s; $p_{wm}(i)$ is the flow pressure, MPa; D_m is the diameter of wellbore, m; ρ is the oil density, kg/m^3; mV is the oil momentum, kg·m/s; θ is the wellbore inclination angle, °; g is the gravitational acceleration, m/s^2.

The conservation of mass principle is derived as Eq. (9):

$$\rho V_m(i)\frac{\pi D_m^2}{4}-\rho V_m(i+\Delta L_m)\frac{\pi D_m^2}{4}=\rho V_{mr}(i)\phi\pi D_m\Delta L_m\tag{9}$$

And then, Eq. (8) is applied to Eq. (9), L is infinitely close to zero and each physical quantity is measured in mining units, the wellbore flow drop model Δp_{wm} can be obtained by obtaining the limit, as Eq. (10):

$$\begin{aligned}\Delta p_{wm}&=\sum_{i=1}^{M}\Delta p_{wm}(i)\\&=\sum_{i=1}^{M}\frac{\rho L}{M}\left\{\frac{2.7146\times10^{-14}}{D_m^5}\left[f_0(1-\phi)+C_f f_0\phi\right][2q_{ml}(i)-Q_{mr}(i)]^2\right.\\&\quad\left.+\frac{2.1717\times10^{-13}MQ_{mr}(i)}{LD_m^4}[2q_{ml}(i)-Q_{mr}(i)]+\frac{\rho g\sin\theta}{10^3}\right\}\end{aligned}\tag{10a}$$

$$Q_{mr}(i,n\Delta t)=\int_0^{\Delta L_m}q_{mr}(i,n\Delta t)\tag{10b}$$

where, $\tau_{w1}(i)$ is friction resistance of wellbore, $\tau_{w1}(i)=\frac{f_0\rho V_m^2(i)}{8}$, f_0 is friction efficient; $\tau_{w2}(i)$ is the friction between radial flow and axial flow, $\tau_{w2}(i)=\frac{C_f f_0\rho V^2(i)}{8}$, C_f is the correction coefficient for friction resistance when there is radial inflow; ρ is the fluid density, g/cm^3; $q_{ml}(i)$ is the upstream flow of the i-th segment, m^3/d; $Q_{mr}(i)$ is the reservoir radial inflow of i-th segment, m^3/d.

(3) Coupling model of reservoir percolation and wellbore variable mass flow

In the bottom water reservoir, the wellbore variable mass flow and reservoir percolation are linked flow processes that are dependent on one another. Using the principle of pressure continuity and the relationship between pressure and flow rate, the coupling model for the i-th element at any time $n\Delta t\,(n\geq1)$ can be established as shown in Eq. (11):

Suppose the oil-water interface pressure is p_e, the mathematical model of radial flow rate and flow pressure along the production section of multilateral horizontal well in the bottom water reservoir can be obtained as shown in Eq. (12):

$$\Delta p(i,n\Delta t)=p_{\mathrm{i}}-p_{\mathrm{wm}}(i,n\Delta t)=\Delta L_{\mathrm{m}}\sum_{i=1}^{M}q_{\mathrm{mr}}(i,n\Delta t)F_i(x_{\mathrm{w}},y_{\mathrm{w}},z_{\mathrm{w}},\Delta t)+\Delta L_{\mathrm{m}}\sum_{i=1}^{M}\sum_{s=1}^{n-1}q_{\mathrm{mr}}(i,s\Delta t)\{F_i[x_{\mathrm{w}},y_{\mathrm{w}},z_{\mathrm{w}},(n-s+1)\Delta t]$$
$$-F_i[x_{\mathrm{w}},y_{\mathrm{w}},z_{\mathrm{w}},(n-s)\Delta t]\}+\Delta L_{\mathrm{bj}}\sum_{j=1}^{N}\sum_{k=1}^{T}q_{\mathrm{br}}(j,k,n\Delta t)F_{j,k}(x_{\mathrm{w}},y_{\mathrm{w}},z_{\mathrm{w}},\Delta t)$$
$$+\Delta L_{\mathrm{bj}}\sum_{j=1}^{N}\sum_{k=1}^{T}\sum_{s=1}^{n-1}q_{\mathrm{br}}(j,k,s\Delta t)\left\{F_{j,k}[x_{\mathrm{w}},y_{\mathrm{w}},z_{\mathrm{w}},(n-s+1)\Delta t]-F_{j,k}[x_{\mathrm{w}},y_{\mathrm{w}},z_{\mathrm{w}},(n-s)\Delta t]\right\} \tag{11}$$

where, p_{wm} is the main wellbore pressure drop, MPa; p_{wb} is the branch wellbore pressure drop, MPa.

By developing corresponding procedures and using iterative methods to solve the model, the production of multilateral horizontal wells can be calculated by Eq. (13)

$$\begin{bmatrix}\mathbf{A}_{\sum_{j=1}^{N}T\times\sum_{j=1}^{N}T} & \mathbf{B}_{\sum_{j=1}^{N}T\times M}\\ \mathbf{C}_{M\times\sum_{j=1}^{N}T} & \mathbf{D}_{M\times M}\end{bmatrix}\begin{bmatrix}\int_0^{\Delta L_{\mathrm{b1}}}q_{\mathrm{br}}(1,1)\\ \int_0^{\Delta L_{\mathrm{b1}}}q_{\mathrm{br}}(1,2)\\ \cdot\\ \cdot\\ \int_0^{\Delta L_{\mathrm{b1}}}q_{\mathrm{br}}(1,T_1)\\ \cdot\\ \cdot\\ \int_0^{\Delta L_{\mathrm{bN}}}q_{\mathrm{br}}(N,T_N)\\ \int_0^{\Delta L_{\mathrm{m}}}q_{\mathrm{mr}}(1)\\ \int_0^{\Delta L_{\mathrm{m}}}q_{\mathrm{mr}}(2)\\ \cdot\\ \cdot\\ \int_0^{\Delta L_{\mathrm{m}}}q_{\mathrm{mr}}(M)\end{bmatrix}=\frac{1.842\times10^{-3}\mu}{hk_{\mathrm{h}}L}\begin{bmatrix}p_{\mathrm{e}}-p_{\mathrm{wb}}(1,1)\\ p_{\mathrm{e}}-p_{\mathrm{wb}}(1,2)\\ \cdot\\ \cdot\\ p_{\mathrm{e}}-p_{\mathrm{wb}}(1,T_1)\\ \cdot\\ \cdot\\ p_{\mathrm{e}}-p_{\mathrm{wb}}(N,T_N)\\ p_{\mathrm{e}}-p_{\mathrm{wm}}(1)\\ p_{\mathrm{e}}-p_{\mathrm{wm}}(2)\\ \cdot\\ \cdot\\ p_{\mathrm{e}}-p_{\mathrm{wm}}(M)\end{bmatrix} \tag{12a}$$

$$\mathbf{A}_{\sum_{j=1}^{N}T\times\sum_{j=1}^{N}T}=\begin{bmatrix}p_{b(1,1)(1,1)} & \cdot & p_{b(1,1)(1,T_1)} & \cdot & p_{b(1,1)(N,T_N)}\\ \cdot & \cdot & \cdot & \cdot & \cdot\\ p_{b(1,T_1)(1,1)} & \cdot & p_{b(1,T_1)(1,T_1)} & \cdot & p_{b(1,T_1)(N,T_N)}\\ p_{b(2,1)(1,1)} & \cdot & p_{b(N,T_N)(1,T_1)} & \cdot & p_{b(N,T_N)(N,T_N)}\end{bmatrix}\mathbf{B}_{\sum_{j=1}^{N}T\times M}=\begin{bmatrix}p_{b(1,1)m(1)} & p_{b(1,1)m(2)} & \cdot & p_{b(1,1)m(M)}\\ \cdot & \cdot & \cdot & \cdot\\ p_{b(1,T_1)m(1)} & p_{b(1,T_1)m(2)} & \cdot & p_{b(1,T_1)m(M)}\\ \cdot & \cdot & \cdot & \cdot\\ p_{b(N,T_N)m(1)} & p_{b(N,T_N)m(2)} & \cdot & p_{b(N,T_N)m(M)}\end{bmatrix}$$

$$\mathbf{C}_{M\times\sum_{j=1}^{N}T}=\begin{bmatrix}p_{m(1)b(1,1)} & \cdot & p_{m(1)b(1,T_1)} & \cdot & p_{m(1)b(N,T_N)}\\ p_{m(2)b(1,1)} & \cdot & p_{m(2)b(1,T_1)} & \cdot & p_{m(2)b(N,T_1)}\\ \cdot & \cdot & \cdot & \cdot & \cdot\\ p_{m(M)b(1,1)} & \cdot & p_{m(M)b(1,T_1)} & \cdot & p_{m(M)b(N,T_N)}\end{bmatrix}\mathbf{D}_{M\times M}=\begin{bmatrix}p_{m(1)m(1)} & p_{m(1)m(2)} & \cdot & p_{m(1)m(M)}\\ p_{m(2)m(1)} & p_{m(2)m(2)} & \cdot & p_{m(2)m(M)}\\ \cdot & \cdot & \cdot & \cdot\\ p_{m(M)m(1)} & p_{m(M)m(2)} & \cdot & p_{m(M)m(M)}\end{bmatrix} \tag{12b}$$

Table 2
Basic parameters of reservoir, fluid and wellbore.

Parameters	Value	Parameters	Value
Reservoir thickness h, m	13.44	Oil density ρ_o, g·cm^{-3}	0.9
Reservoir horizontal/vertical permeability k_h/k_v, $10^{-3}\mu m^2$	1000/600	Distance between the wellbore and the lower boundary z_w, m	3.42
Porosity	0.37	Main wellbore length L, m	400
Reservoir total compressibility coefficient C_t, MPa^{-1}	1.25×10^{-3}	Branch wellbore length L_b, m	150
Reservoir initial pressure p_i, MPa	11.7	Branch angle α, °	20
Oil viscosity μ, mPa·s	50	Wellbore radius r_w, m	0.1

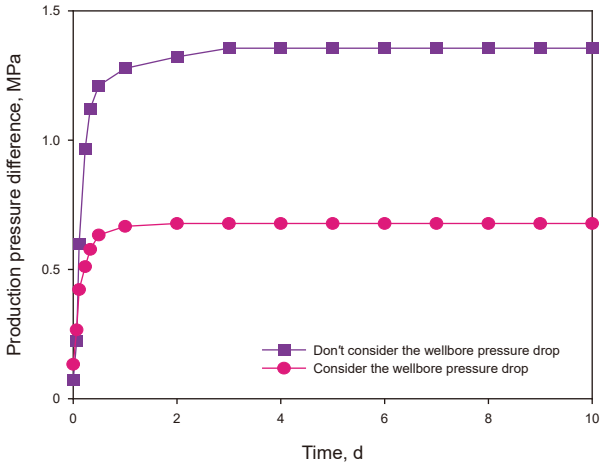

Fig. 2. Pressure difference change curve at heel end of herringbone main wellbore.

$$Q(n\Delta t)=\sum_{i=1}^{M} q_{mr}(i,n\Delta t)+\sum_{j=1}^{N}\sum_{k=1}^{T} q_{br}(j,k,n\Delta t),\ (1\le i\le M,1\le j\le N,1\le k\le T,n\ge 1) \tag{13}$$

Along the multilateral horizontal well's production section, the flow pressure adheres to the relationship shown in Eq. (14):

$$p_{wm}(i,n\Delta t)=p_{wm}(i-1,n\Delta t)+0.5[\Delta p_{wm}(i,n\Delta t)+\Delta p_{wm}(i-1,n\Delta t)],p_{wm}(1,n\Delta t)=p_{wm}(0,n\Delta t)+0.5\Delta p_{wm}(1,n\Delta t),(2\le i\le M+1,n\ge 1) \tag{14}$$

The multi-branch horizontal wells production coupling model is derived based on the point source function, and it is appropriate for arbitrary distribution in three-dimensional reservoir space. The model comprehensive considers all factors, increasing the difficulty and computational complexity of solving the nonlinear equation system. However, using the program developed in this paper and the Newton iteration method, the iterative solution of the model can be quickly completed.

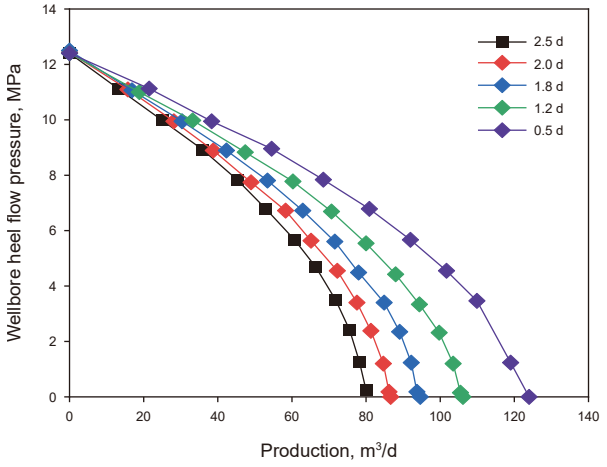

Fig. 3. IPR curve of multilateral horizontal well.

2.2.2. Bottom water breakthrough dynamic model of multilateral horizontal well

Model II is the bottom water breakthrough dynamic model of multilateral horizontal well. Based on the original oil-water interface, define the oil phase potential function as Eq. (15):

$$\Phi(x,y,z)=p_e-p(x,y,z)-\rho_o gH \tag{15}$$

At the front of the water ridge, the potential function at the oil-water interface is shown as Eq. (16):

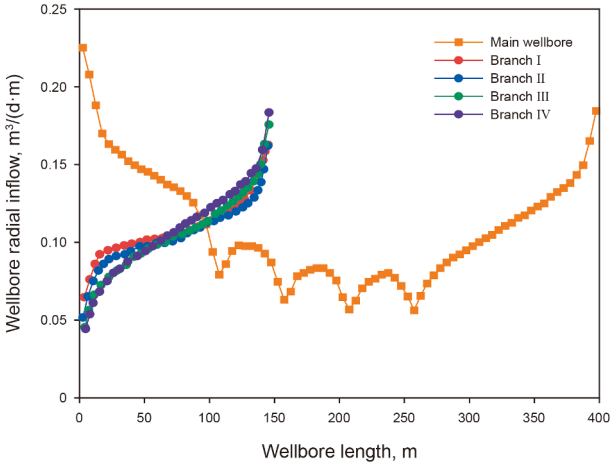

Fig. 4. Radial inflow distribution of multilateral horizontal well wellbores.

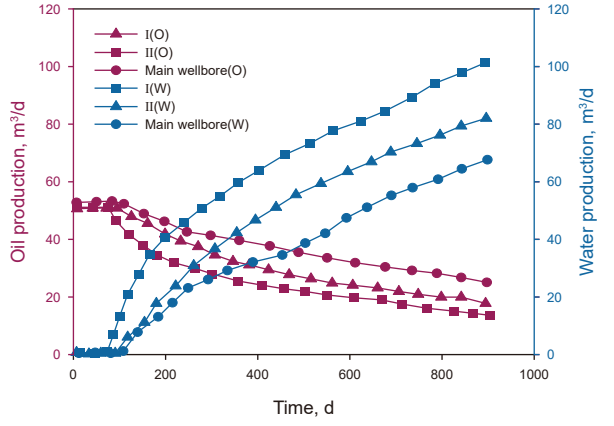

Fig. 5. The variations of water (W) and oil production (O) over time.

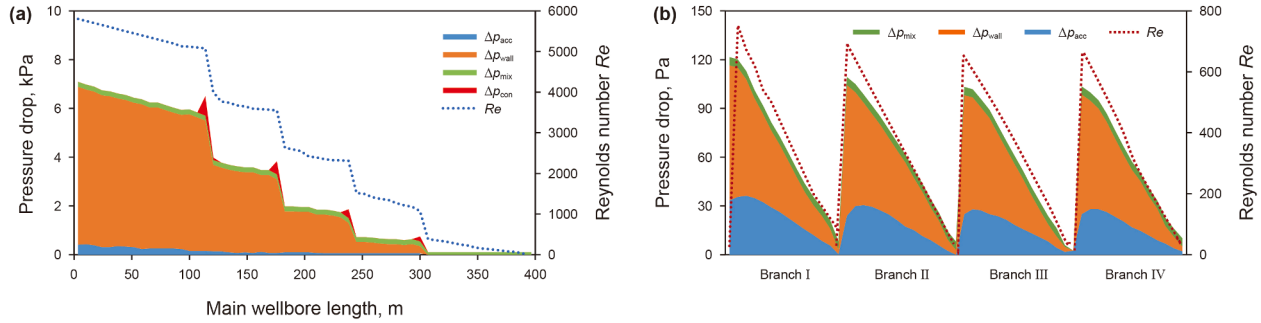

Fig. 6. Reynolds number and pressure drop composition of main wellbore. (**a**) Main wellbore; (**b**) branch wellbore. Here, Δp_{mix} is mixed pressure drop, kPa; Δp_{acc} is acceleration pressure drop, kPa; Δp_{wall} is friction pressure drop, kPa; Δp_{con} is convergence pressure drop, kPa.

$$\Phi_f(x,y,z) = p_e - p(x,y,z) - \rho_o g H - (\rho_w - \rho_o) g H_f \tag{16}$$

where, H is the oil column height, m; H_f is the water ridge front height, m; ρ_w is the water density, g/cm^3; ρ_o is the oil density, g/cm^3; Φ is the oil phase potential function; Φ_f is the oil phase potential function at the oil-water interface; p_e is the oil-water interface pressure, MPa.

Next, the distribution of water breakthrough time at various positions is obtained by using the numerical integration method, and the calculation formula is obtained as Eq. (17):

Water breakthrough time t_b(d):

$$t_b = 1.1574 \times 10^{-2} \frac{\mu\phi(1 - S_{wc} - S_{or})}{k_v} \int_0^{z_w} \frac{dz}{\partial\Phi_f(x,0,z)/\partial z} \tag{17a}$$

Water cresting rising speed v (in m/s):

$$v = 10^{-3} \times \frac{k_v}{\mu\phi(1 - S_{wc} - S_{or})} \frac{\partial\Phi_f(x,0,z)}{\partial z} \tag{17b}$$

where, $\partial\Phi_f(x,0,z)/\partial z$ is the potential gradient at any point on the yz plane in the reservoir, MPa/m; S_{wc} is irreducible water saturation; S_{or} is residual oil saturation; t_b is the water breakthrough time, d; v is the water cresting rising speed, m/s.

The multilateral horizontal well bottom water breakthrough dynamic model is derived based on the coupling relationship between reservoir percolation and wellbore variable-mass flow in bottom water reservoirs. It takes into account the coupling relationship between wellbore variable-mass flow and reservoir percolation, as well as wellbore pressure drop and branch interference. It can predict the water breakthrough time and the sequence of water breakthrough locations for multilateral horizontal wells with arbitrary spatial distribution in bottom water reservoirs. The model's foundation in Darcy's law makes it appropriate for medium-high permeability reservoirs, particularly for predicting the water breakthrough performance and production dynamics of bottom water reservoirs.

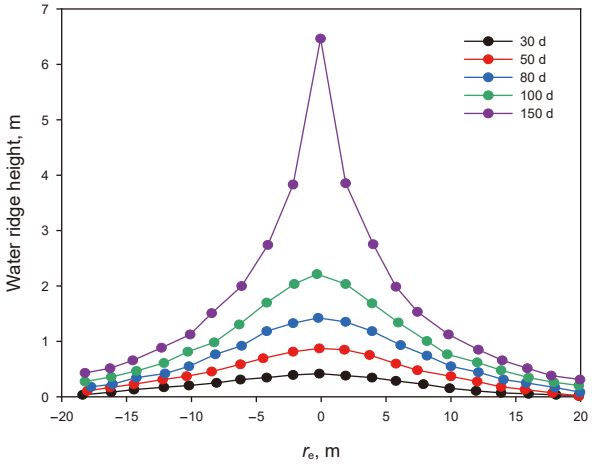

Fig. 7. Water ridge profile morphology at different times.

3. Analysis of results

Using the multilateral horizontal well as the research object, which is currently producing and has extensive production data recorded in the extremely shallow seawater of Shengli Oilfield Chengbei region. The multilateral horizontal well was put into production in March 2020, and the oil distribution is comparatively stable with bottom water energy replenishment beneath the oil layer. When the main wellbore and branch wellbore are producing concurrently, utilizing the coupled model developed in this paper to study the inflow dynamics, pressure drop composition, productivity and water breakthrough dynamics characteristics. The basic parameters of reservoir, fluid, and wellbore are shown (Table 2).

3.1. Analysis of inflow dynamic characteristics

The main wellbore production section's production pressure difference variation curves over time is depicted. After a brief production period of about 0.6 h, the multilateral horizontal well's pressure differential stops varying with production time, indicating that the reservoir's fluid flow progressively changes from an

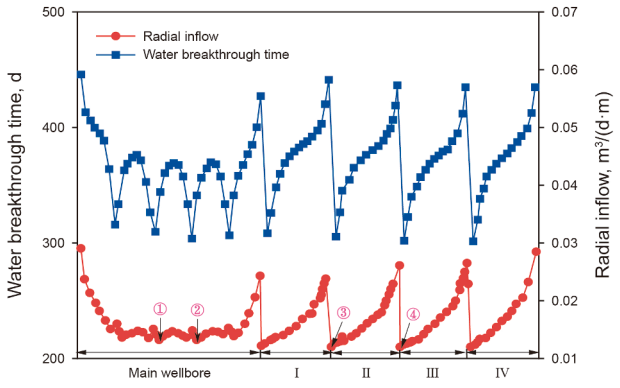

Fig. 8. Distribution curve of flow and breakthrough time of multilateral horizontal well.

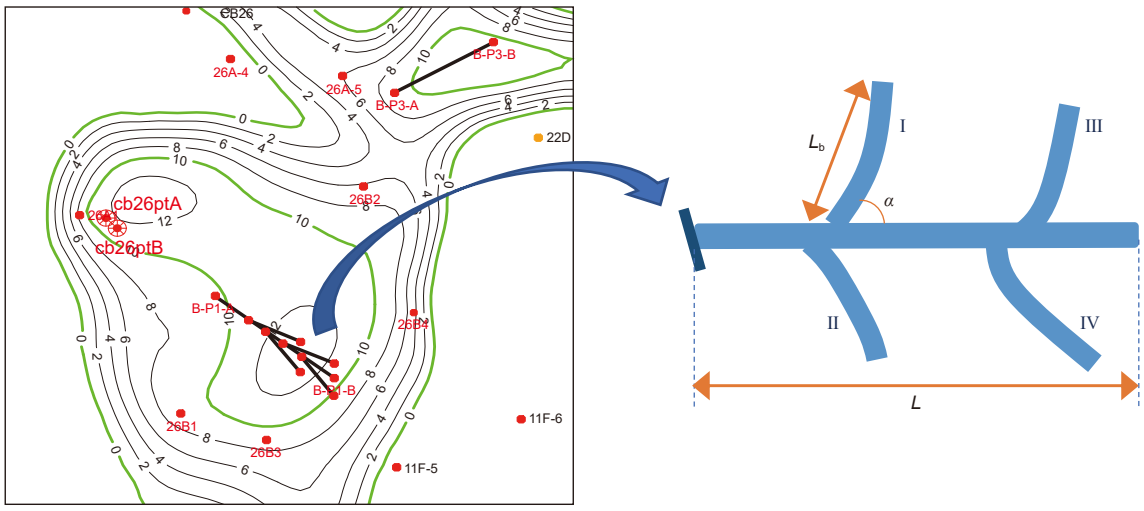

Fig. 9. Multilateral horizontal well trajectory model in the reservoir.

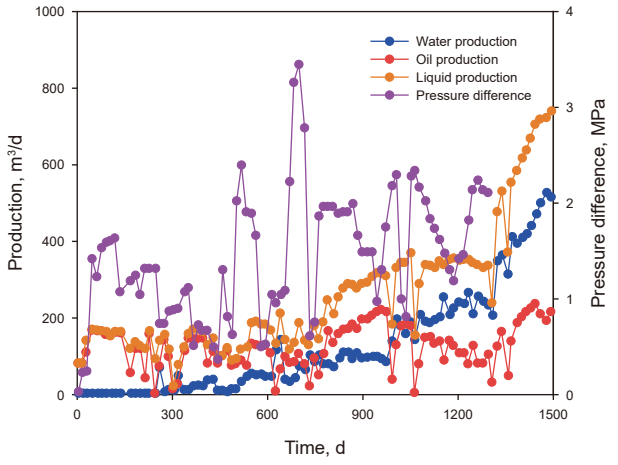

Fig. 10. Production curves of multilateral horizontal well.

unstable to a stable flow stage with a steady bottom water pressure supply. When the pressure drop inside the wellbore is taken into account, the production pressure difference of the wellbore increases (Fig. 2). This results in an excessively high production prediction for the multilateral horizontal well, therefore, the wellbore pressure drops cannot be ignored when establish the production model.

Production gradually decreases before plateauing as production time increases. Because of the flow's initial restriction to the vicinity of the multilateral horizontal well and its highly unstable flow state, production fell off dramatically. The pressure waves eventually extend to areas farther away from the reservoir, and the flow tends to level out (Fig. 3).

The main wellbore radial inflow has the characteristic of "low in the middle and high at both ends". Due to the influence of branch convergence causes the interference to be greater at the junction of the main and branch wellbores, which lowers the radial inflow into the wellbore. For branch wellbores, the flow rate gradually increases from the heel end to the toe end, the primary cause is

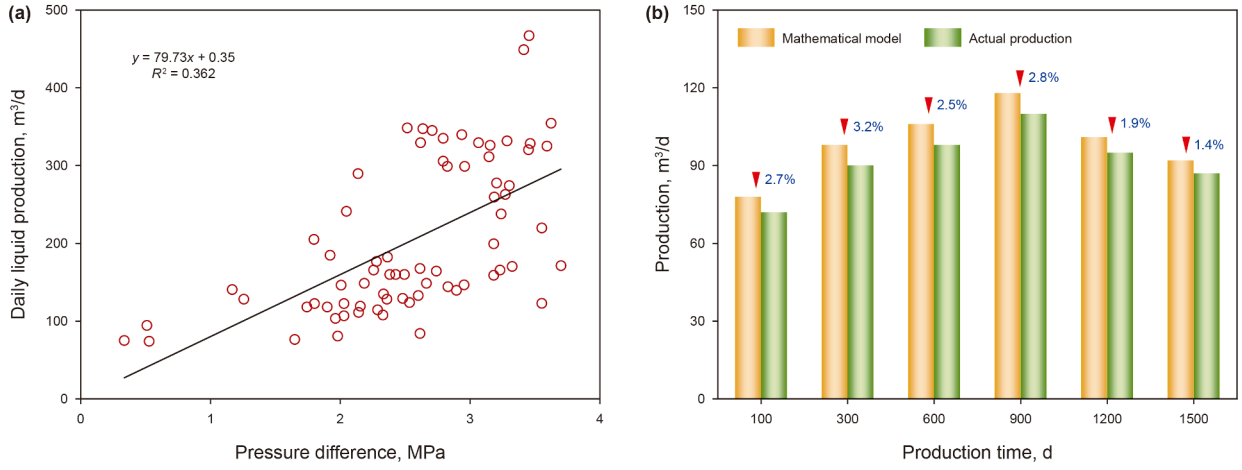

Fig. 11. Production and pressure difference of multilateral horizontal well. (**a**) Regression analysis of production and pressure difference of multilateral horizontal well in actual production. (**b**) Comparison of production at different production time about mathematical mode and actual production.

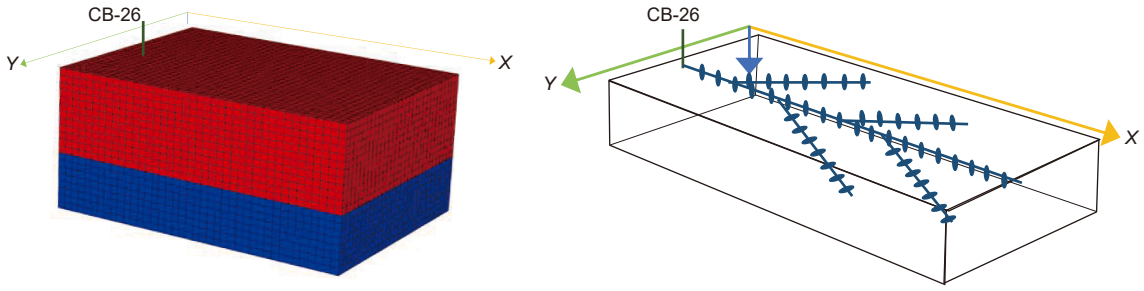

Fig. 12. Numerical simulation model of the multilateral horizontal well.

Table 3
Well completion data.

Parameters	Top measure depth, m	Bottom measure depth, m	Wellbore length, m	Completion method
Main wellbore	1707.0	1913.5	206.5	Slotted liner
	1917.9	2075.5	157.6	
Branch I	1832.4	1983.0	150.6	Open hole
Branch II	1876.3	1976.7	100.4	Open hole
Branch III	1912.6	2061.3	148.7	Open hole
Branch IV	1953.2	2053.7	100.5	Open hole

Table 4
Numerical water parameters.

Water parameters				Connection between water and oil reservoirs					
Depth, m	Initial pressure, MPa	Initial volume, m^3	Water drive index, $m^3/(d\cdot bar)$	Lower I	Upper J	Lower I	Upper J	Lower I	Upper J
2500	27	1.2E+10	1.0E+03	1	75	1	50	67	67

that the branch wellbore's heel end is nearer the main wellbore, which results in increased interference and decreased inflow. The degree of interference to branch wellbores varies depending on the branch position, at the heel end, branch I and II have a higher inflow than branch III and IV, however, at the toe end is opposite (Fig. 4). The variations in water (W) and oil production (O) over time with respect to the main wellbore and branch I, II is depicted. Over time, the water content rises while the oil production steadily declines. The production varies depending on the branch position. Because there is less interference, branch I produces more than branch II (Fig. 5).

3.2. Analysis of wellbore pressure drop composition

The composition of the pressure drop and Reynolds number in the multilateral horizontal well's wellbore (Fig. 6). For the main wellbore, there is a step change in the pressure drop at the branch confluence and a convergence pressure drop because of the convergence of the branch wellbore. The Reynolds number *Re* ($Re = \rho vd/\mu$) jumping increases at the confluence of branches, resulting in a significant increase in frictional pressure drop closely related to Reynolds number. In total pressure drop, friction pressure drop makes up the largest portion (93.1%), followed by

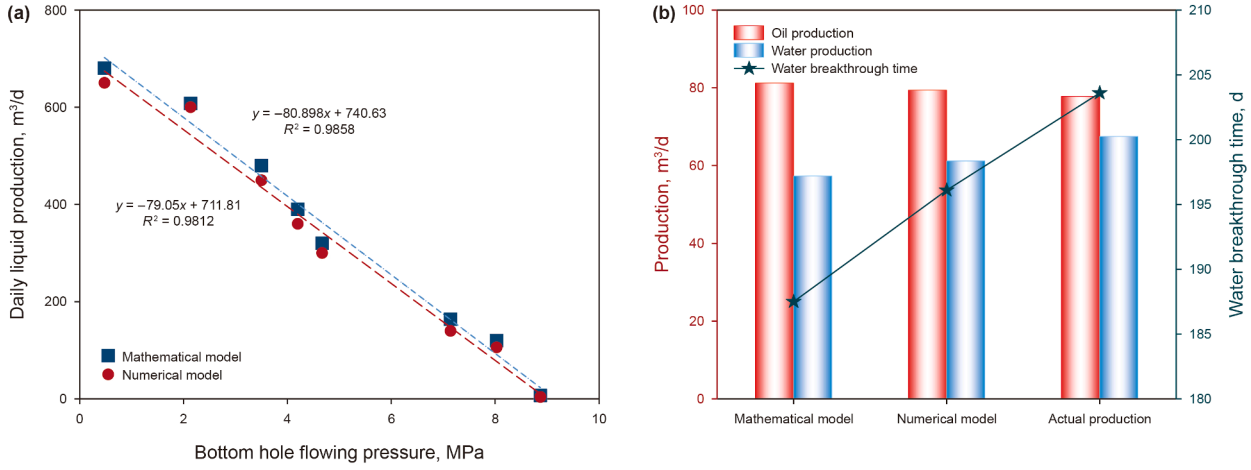

Fig. 13. Comparison of mathematical model and numerical model. (**a**) Relationship between production and pressure difference in mathematical model and numerical model. (**b**) Comparison of production and water breakthrough time.

acceleration pressure drop (5.1%), convergence pressure drop (1.07%), and mixed pressure drop (0.73%) (Fig. 6(a)). For branch wellbores, both the Reynolds number *Re* and the overall pressure drop gradually rise from the toe end to the heel end, most of the pressure drop is caused by friction, followed by acceleration, and the smallest percentage is caused by mixed pressure drop (Fig. 6(b)).

3.3. Analysis of water breakthrough dynamic characteristics

The water ridge's cross-sectional morphology at various time points is depicts. Initially, it rises slowly before accelerating gradually until the water ridge breakthrough the oil well and water is visible (Fig. 7).

The distribution trajectory of the water breakthrough time is comparable to that of the inflow rate, that is, the water breakthrough time earlier at low flow rates. Due to the interference and diversion in the angle area near the confluence of the main wellbore and the branch wellbore, the flow interference is large and the flow rate is low, resulting in a large vertical pressure gradient in the oil reservoir. Therefore, the water ridge rises quickly and the water breakthrough time is short (Fig. 8).

4. Discussion

4.1. Model validation analysis

(1) Field application

Taking the Shengli Oilfield Chengbei block's herringbone branch well CB-26, which has full production data, as the study's subject. By utilizing the actual mining sites production data and numerical simulation methods to confirm the accuracy of the mathematical model which established in this paper. The reservoir has multiple oil, gas, and water systems, the Dongying formations I and II oil lower section are the target layer for development, with a porosity of 27%–31% and an average of 29%, the permeability is 100×10^{-3}–10000×10^{-3} μm^2. The original formation pressure is 10.67 MPa, the layer effective thickness is 18.3 m, the average distance between the wellbore and reservoir is 6.58 m, the effective formation permeability is 3029×10^{-3} μm^2, the anisotropy coefficient is 3.15, and the underground crude oil viscosity is 351 mPa·s. The distribution of the oil layers is comparatively stable and with bottom water energy replenishment below (Fig. 9).

The fluid production, water production, oil production, and pressure difference variation curves of the multilateral horizontal well over production time (Fig. 10).

The regression curve of the relationship among liquid production and pressure difference in actual production. As illustrated, the fluid production is equal to 79.73 × production pressure difference, which the fluid production index is 79.73 m^3/(d·MPa) (Fig. 11(a)). The mathematical model's computed production index is marginally higher than the actual field date. The reason is that all of the branches' production sections were taken into account during the productivity computation in this paper, ignoring the formation damage and wellbore stability. Even though the aforementioned factors might cause some inaccuracies between calculated values and actual production data, it is evident that the difference between the two is less than 4%. If some branch sections do not participate in production, or if oil-water two-phase flow causes a decrease in liquid volume of 4%, the calculated results are basically consistent with the actual results (Fig. 11(b)).

(2) Numerical simulation analysis

The numerical simulation of the bottom water reservoir multilateral horizontal well model is showed, the grid system is 75 × 50 × 67, and the model dimensions (D) are $D_X = 15$ m and $D_Y = 10$ m, the water layer's D_Z ($z = 67$) is 3.42 m, while the oil layer's ($z < 67$) is 10.2 m (Fig. 12). Tables 3 and 4 show the well completion data and numerical water parameters.

According to the productivity coupling model for multilateral horizontal wells developed in this paper, when the bottomhole pressure of the multilateral horizontal well is higher than the bubble point pressure, the relationship curve between fluid production and pressure difference is essentially a straight line, with a fluid production index of 80.898 m^3/(d·MPa), and the fluid production index is 79.05 m^3/(d·MPa) in numerical model (Fig. 13(a)). Between the numerical simulation, the mathematical model and the actual production, the liquid production index has an error of roughly 2.46% and 0.85%, the oil production index has an error of roughly 4.4% and 2.1% (Table .5 and Fig. 13(b)). The reason for the error is that the production dynamic data attained by mathematical model is the single-phase oil recovery, while the numerical simulation and the actual filed data are water & oil two-phase flow, which increases the flow resistance. Furthermore, the lack of consideration for reservoir damage and wellbore stability in the mathematical model may also result in higher computed values. Therefore, this article's computed liquid production index is marginally higher than the numerical simulation data, this indicates that the production model derived from the multilateral horizontal well in this paper is accurate.

The distribution of bottom water breakthrough locations during the numerical simulation process is depicts. The water breakthrough early occurs at the intersection of the main and branch wellbores, then moves on to the middle section of the main wellbore and the heel position of each branch wellbore, at the two ends of the main wellbore and the toe position of each branch wellbore is relatively late, the result is consistent with the theoretical model results (Fig. 14).

4.2. Sensitivity analysis

At present, many scholars have conducted relevant research on the factors that affecting the multilateral horizontal wells productivity, but there are relatively few studies that consider the intrinsic relationships between influencing factors. To maximize the benefits of multilateral horizontal well production, the reservoir flow coupling model developed in this paper is utilized to determine productivity and water breakthrough time under various branch parameters, to optimize multilateral horizontal well shape, and accurately direct multilateral horizontal well design.

The smaller the diameter of the wellbore, the more difficult it is for fluid to flow inside the wellbore, resulting in a greater accumulation pressure drop in the wellbore, and the difference in production caused by the wellbore pressure drop is greater (Fig. 15). The cumulative pressure drop in the wellbore increases with decreasing oil viscosity and the difference in production caused by the wellbore pressure drop is greater. This is because the

Table 5
Error analysis between mathematical model, numerical model and actual data.

Parameters	Oil production, m^3/d	Water production, m^3/d	Water breakthrough time, d	Oil production error, %
Mathematical model	81.2	57.3	187.5	4.4
Numerical model	79.4	61.2	196.1	2.1
Actual data	77.8	67.5	203.6	

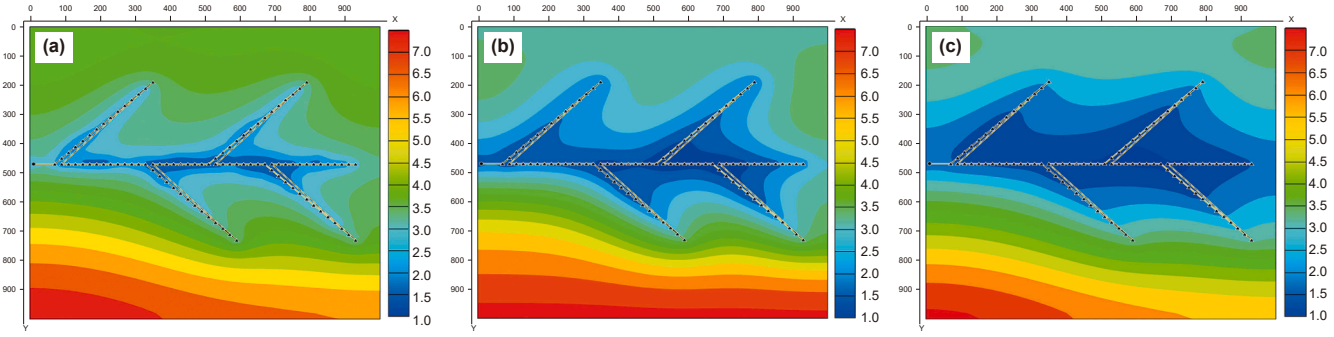

Fig. 14. Bottom water breakthrough locations distribution at various time. (**a**) 172 d; (**b**) 186 d; (**c**) 215 d.

main wellbore's flow rate increases more quickly with decreasing viscosity, and the pressure drop in the wellbore gradually increases. Therefore, the pressure drop in the production section should be considered for low viscosity wells (Fig. 16).

As the branch angle increases, the distance between the branch and main wellbores increases, leads to the interference decreases and the oil production rises. However, the increase in oil production gradually declines. When the branch angle is between 75° and 90°, the two production curves nearly coincide, and the interference between the wellbores barely varies as the branch angle changes (Fig. 17(a)). The water breakthrough time gradually delays as the branch angle increases, the increase in water breakthrough time increases more when the branch angle is less than 30°, and it slows down when the branch angle exceeds 30° (Fig. 17(b)). The reason is that the interference between branches increases as the branch wellbore gets closer to the main wellbore, the branch angle is a sensitive factor for the water breakthrough time.

The oil production rises with increasing branch length, but the rate of increase falls. This is because a longer branch may cause more interference between the main wellbore and the branch wellbore, which would lower their production. Compared to branch angle, branch length has a greater effect on oil production (Fig. 18(a)). With increasing branch length, the water breakthrough time gradually rises. The rationale is that, under constant production conditions, longer wellbores suppress the ridge of bottom water and delay the water breakthrough time by decreasing the potential difference that causes the bottom water to rise (Fig. 18(b)).

The oil production rises initially and then falls as the number of branches increases. This is because a greater number of branches causes more interference between the branch and main wellbores, which lowers production more than an increase in branches. In the later stage of mining, the oil production declines when there are more than 5 branches. The impact of branch numbers on oil production is lower than that of branch length (Fig. 19(a)). The cumulative production rises as the number of branches rises, but the increase in production slows down as a result of wellbores interference. The bottom water in the 5 branches' multilateral horizontal well breakthrough sooner than the others. That's because of the early breakthrough of the branch wellbore that is the furthest away from the main wellbore of the 5-branched multilateral

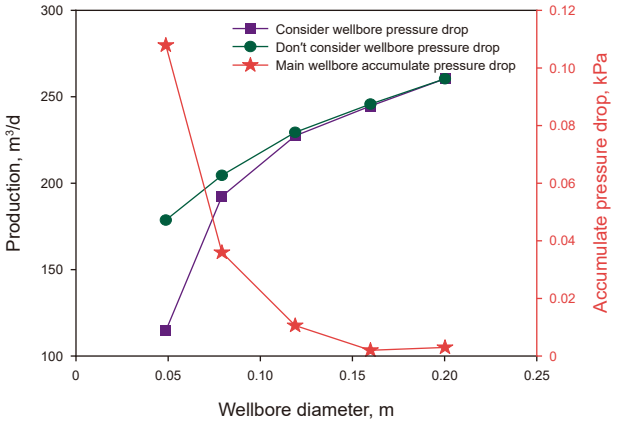

Fig. 15. The effect of wellbore diameter on pressure drop and production.

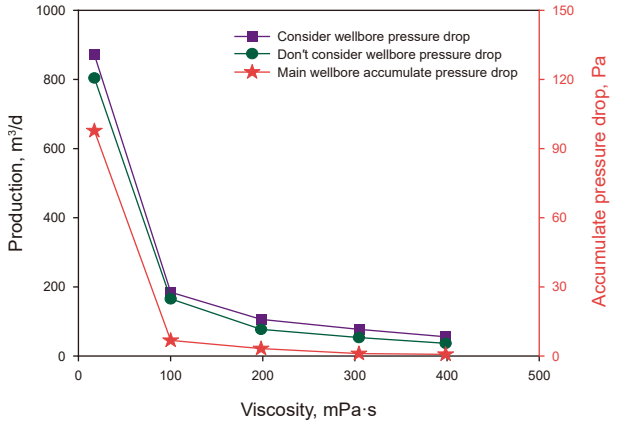

Fig. 16. The effect of viscosity on pressure drop and production.

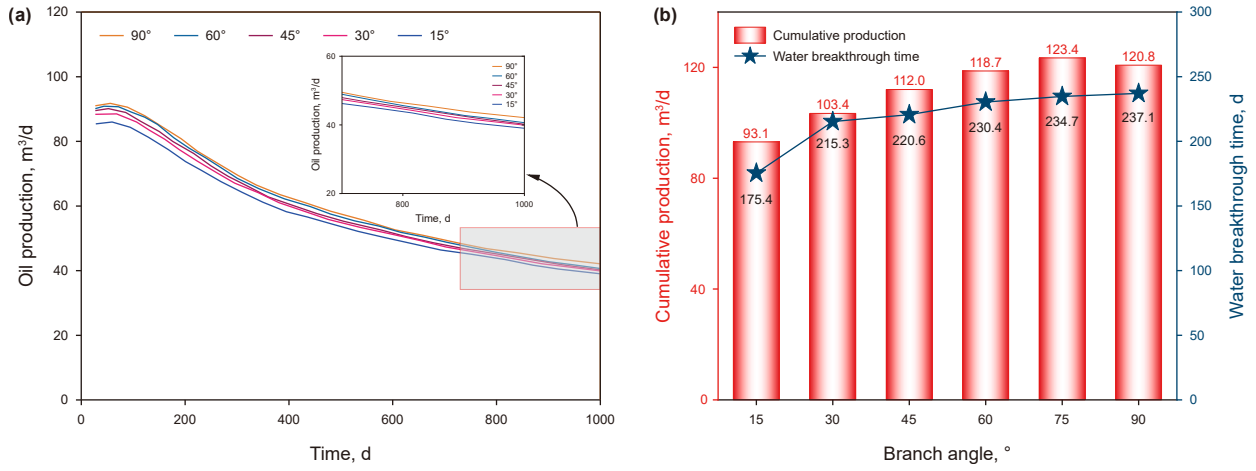

Fig. 17. The relationship among production and water breakthrough time at different branch angle. (**a**) Oil production vs branch angle at different production time. (**b**) Production and water breakthrough time vs branch angle.

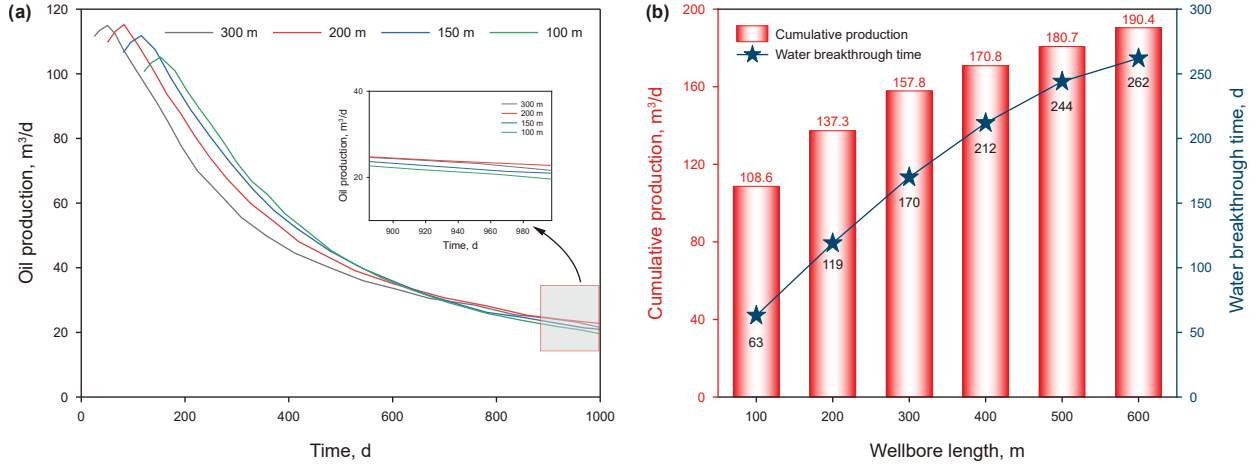

Fig. 18. The relationship among production and water breakthrough time at different branch length. (**a**) Oil production vs branch length at different production time. (**b**) Production and water breakthrough time vs branch length.

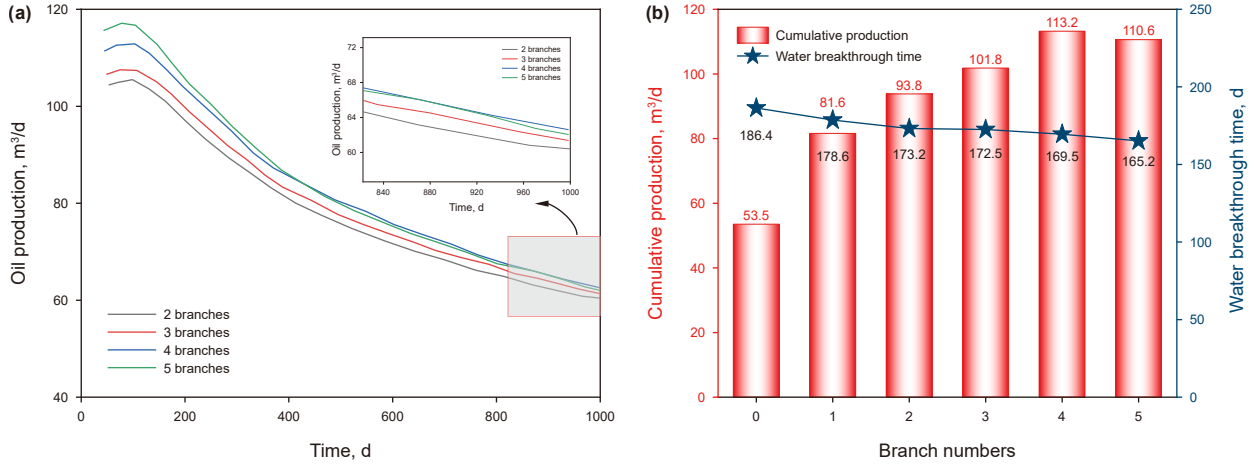

Fig. 19. The relationship among production and water breakthrough time at different branch numbers. (**a**) Oil production vs branch numbers at different production time. (**b**) Production and water breakthrough time vs branch numbers.

horizontal well, while the other wellbore breaks early at the main wellbore's heel (Fig. 19(b)).

5. Conclusions

In this paper, a coupled model of predicting dynamic production and water breakthrough for multilateral horizontal well with arbitrary three-dimensional spatial distribution is proposed, which can be used to calculate and predict the production, breakthrough time and recovery efficiency of multilateral horizontal well, and it supplies strong technical support for further development and EOR of bottom water reservoir and actual oil field productions.

(1) A coupled flow model of multilateral horizontal well considering the branches interference and variable mass flow is proposed, which can predict dynamic production, flow profiles and water breakthrough time, and describe pressure drop components change and flow characteristics as well as the water breakthrough time and position.
(2) The wellbore inflow profile represents a characteristic of "low in the middle and high at both ends" on account of branches interference. The pressure drop is mainly affected by friction, and other pressure drop types are acceleration pressure drop, convergence pressure drop and mixed pressure drop.
(3) The breakthrough time is prior at junction of main wellbore and branch wellbores with low flow rates, then spreads to the middle position of main wellbore and trailing position of each branch wellbore. The branch length has a significant impact on breakthrough time, then, the branch numbers and the branch angle.

CRediT authorship contribution statement

Chun-Xue Cui: Writing – review & editing, Writing – original draft, Visualization, Supervision, Methodology, Investigation, Formal analysis, Data curation, Conceptualization. **Xiao-Long Chai:** Writing – review & editing, Resources, Project administration, Methodology, Conceptualization. **Yue-Wu Liu:** Resources, Project administration, Methodology, Conceptualization. **Zhi-Jun Zhou:** Writing – review & editing, Resources, Project administration, Conceptualization. **Guo-Qing Zhang:** Visualization, Investigation, Formal analysis, Data curation. **Leng Tian:** Resources, Funding acquisition, Conceptualization.

Declaration of interest statement

The authors declare that they have no conflict of interest related to this article.

Acknowledgments

The authors would like to acknowledge the funding by the project (51974329) sponsored by the National Natural Science Foundation of China and the project (2024ZD1406601) sponsored by the National Major Science and Technology Projects of China.

Appendix

The flow pattern of fluids in infinite reservoir flowing to any perforation in the main wellbore conforms to the three-dimensional partial differential equation of seepage flow as Eq. (1):

$$k_x\frac{\partial^2 p}{\partial x^2}+k_y\frac{\partial^2 p}{\partial y^2}+k_z\frac{\partial^2 p}{\partial z^2}=\phi\mu C_t\frac{\partial p}{\partial t} \tag{A.1}$$

Point source solution in the reservoir is

$$\Delta p(x,y,z,t)=\frac{\phi}{8[\pi(t-\tau)]^{3/2}\sqrt{\eta_x\eta_y\eta_z}}\exp\left[-\frac{(x-x')^2}{4\eta_x(t-\tau)}-\frac{(y-y')^2}{4\eta_y(t-\tau)}-\frac{(z-z')^2}{4\eta_z(t-\tau)}\right] \tag{A.2}$$

$$x_D=\frac{x}{L},y_D=\frac{y}{L},z_D=\frac{z}{L}\sqrt{\frac{k_v}{k_h}},t_D=\frac{3.6\eta_r}{L^2}t=\frac{3.6k_h}{\varphi C_t\mu L^2}t \tag{A.3}$$

Attain the solution with dimensionless:

$$\Delta p(x_D,y_D,z_D,t_D)=\frac{3.6^{3/2}\varphi}{8\pi^{3/2}L^3(t_D-\tau_D)^{3/2}\sqrt{k_h/k_v}}\exp\left[-\frac{R_D^2}{4(t_D-\tau_D)}\right] \tag{A.4}$$

where, $R_D^2=3.6(x_D-x'_D)^2+(y_D-y'_D)^2+(z_D-z'_D)^2$.

The point source in Laplace domain:

$$\Delta p(x_D,y_D,z_D,s)=\frac{3.6^{3/2}\varphi}{4\pi L^3R_D\sqrt{k_v/k_h}}\exp\left(-R_D\sqrt{s}\right) \tag{A.5}$$

$$\overline{\Delta p}(x_D,y_D,z_D,t_D)=\frac{\sqrt{3.6}}{4\eta_r\pi L\sqrt{k_v/k_h}}\int_0^{t_D}\frac{\varphi(\tau)}{2\pi^{1/2}(t_D-\tau_D)^{3/2}}\exp\left[-\frac{R_D^2}{4(t_D-\tau_D)}\right]d\tau_D \tag{A.6}$$

where $\varphi(t)=\frac{1.157\times10^{-2}q}{\phi C_t}$.

According to the convolution theorem:

$$f*g=\int_0^t f(\tau)g(t-\tau)d\tau \tag{A.7}$$

$$L[f*g]=\bar{f}(s)\bar{g}(s) \tag{A.8}$$

Point source solution for infinite reservoirs:

$$\overline{\Delta p}(x_D, y_D, z_D, s) = \frac{1.842 \times 10^{-3}\sqrt{3.6}\mu\overline{q}(s)}{2L\sqrt{k_r k_h}} \frac{\exp(-R_D\sqrt{s})}{R_D} \tag{A.9}$$

Using the mirror reaction method:

$$\begin{aligned}
\overline{\Delta p}(x_D, y_D, z_D, s) = {} & \frac{1.842 \times 10^{-3}\sqrt{3.6}\mu}{2L\sqrt{k_h k_v}}\overline{q}(s) \sum_{k=-\infty}^{k=+\infty} \left\{ \frac{\exp\left[-\sqrt{s}\sqrt{3.6}\sqrt{(x_D - x_{wD})^2 + (y_D - y_{wD})^2 + (z_D - z_{wD} - 2\cdot 2nh_D)^2}\right]}{\sqrt{3.6\sqrt{(x_D - x_{wD})^2 + (y_D - y_{wD})^2 + (z_D - z_{wD} - 2\cdot 2nh_D)^2}}} \right. \\
& + \frac{\exp\left[-\sqrt{s}\sqrt{3.6}\sqrt{(x_D - x_{wD})^2 + (y_D - y_{wD})^2 + (z_D + z_{wD} - 2\cdot 2nh_D)^2}\right]}{\sqrt{3.6\sqrt{(x_D - x_{wD})^2 + (y_D - y_{wD})^2 + (z_D + z_{wD} - 2\cdot 2nh_D)^2}}} \\
& \left. - \frac{\exp\left[-\sqrt{s}\sqrt{3.6}\sqrt{(x_D - x_{wD})^2 + (y_D - y_{wD})^2 + [z_D - z_{wD} - 2\cdot(2n+1)h_D]^2}\right]}{\sqrt{3.6\sqrt{(x_D - x_{wD})^2 + (y_D - y_{wD})^2 + [z_D - z_{wD} - 2\cdot(2n+1)h_D]^2}}} \right\} \\
= {} & \frac{1.842 \times 10^{-3}\sqrt{3.6}\mu}{2L\sqrt{k_v k_h}}\overline{q}(s) \sum_{n=-\infty}^{n=+\infty} (-1)^n \left\{ \frac{\exp\left[-\sqrt{s}\sqrt{3.6}\sqrt{(x_D - x_{wD})^2 + (y_D - y_{wD})^2 + (z_D - z_{wD} - 2nh_D)^2}\right]}{\sqrt{3.6\sqrt{(x_D - x_{wD})^2 + (y_D - y_{wD})^2 + (z_D - z_{wD} - 2nh_D)^2}}} \right. \\
& \left. - \frac{\exp\left[-\sqrt{s}\sqrt{3.6}\sqrt{(x_D - x_{wD})^2 + (y_D - y_{wD})^2 + (z_D + z_{wD} - 2nh_D)^2}\right]}{\sqrt{3.6\sqrt{(x_D - x_{wD})^2 + (y_D - y_{wD})^2 + (z_D + z_{wD} - 2nh_D)^2}}} \right\}
\end{aligned} \tag{A.10}$$

where

$$\begin{aligned}
& \sum_{n=-\infty}^{n=+\infty} (-1)^n \left\{ \frac{\exp\left[-\sqrt{s}\sqrt{3.6}\sqrt{(x_D - x_{wD})^2 + (y_D - y_{wD})^2 + (z_D - z_{wD} - 2nh_D)^2}\right]}{\sqrt{3.6}\sqrt{(x_D - x_{wD})^2 + (y_D - y_{wD})^2 + (z_D - z_{wD} - 2nh_D)^2}} \right\} \\
& + \sum_{n=-\infty}^{n=+\infty} \frac{\exp\left[-\sqrt{s}\sqrt{3.6}\sqrt{(x_D - x_{wD})^2 + (y_D - y_{wD})^2 + (z_D - z_{wD} - 2nh_D)^2}\right]}{\sqrt{3.6}\sqrt{(x_D - x_{wD})^2 + (y_D - y_{wD})^2 + (z_D - z_{wD} - 2nh_D)^2}} \\
& = 2\sum_{n=-\infty}^{n=+\infty} \frac{\exp\left[-\sqrt{s}\sqrt{3.6}\sqrt{(x_D - x_{wD})^2 + (y_D - y_{wD})^2 + (z_D - z_{wD} - 2\cdot 2nh_D)^2}\right]}{\sqrt{3.6}\sqrt{(x_D - x_{wD})^2 + (y_D - y_{wD})^2 + (z_D - z_{wD} - 2\cdot 2nh_D)^2}}
\end{aligned} \tag{A.11}$$

and

$$\begin{aligned}&\sum_{n=-\infty}^{n=+\infty}(-1)^n\left\{\frac{\exp\left[-\sqrt{s}\sqrt{3.6}\sqrt{(x_{\mathrm{D}}-x_{\mathrm{wD}})^2+(y_{\mathrm{D}}-y_{\mathrm{wD}})^2+(z_{\mathrm{D}}+z_{\mathrm{wD}}-2nh_{\mathrm{D}})^2}\right]}{\sqrt{3.6}\sqrt{(x_{\mathrm{D}}-x_{\mathrm{wD}})^2+(y_{\mathrm{D}}-y_{\mathrm{wD}})^2+(z_{\mathrm{D}}+z_{\mathrm{wD}}-2nh_{\mathrm{D}})^2}}\right\}\\&+\sum_{n=-\infty}^{n=+\infty}\frac{\exp\left[-\sqrt{s}\sqrt{3.6}\sqrt{(x_{\mathrm{D}}-x_{\mathrm{wD}})^2+(y_{\mathrm{D}}-y_{\mathrm{wD}})^2+(z_{\mathrm{D}}+z_{\mathrm{wD}}-2nh_{\mathrm{D}})^2}\right]}{\sqrt{3.6}\sqrt{(x_{\mathrm{D}}-x_{\mathrm{wD}})^2+(y_{\mathrm{D}}-y_{\mathrm{wD}})^2+(z_{\mathrm{D}}+z_{\mathrm{wD}}-2nh_{\mathrm{D}})^2}}\\&=2\sum_{n=-\infty}^{n=+\infty}\frac{\exp\left[-\sqrt{s}\sqrt{3.6}\sqrt{(x_{\mathrm{D}}-x_{\mathrm{wD}})^2+(y_{\mathrm{D}}-y_{\mathrm{wD}})^2+(z_{\mathrm{D}}+z_{\mathrm{wD}}-2\cdot2nh_{\mathrm{D}})^2}\right]}{\sqrt{3.6}\sqrt{(x_{\mathrm{D}}-x_{wD})^2+(y_{\mathrm{D}}-y_{\mathrm{wD}})^2+(z_{\mathrm{D}}+z_{\mathrm{wD}}-2nh_{\mathrm{D}})^2}}\end{aligned}\tag{A.12}$$

The pressure drop can be written as

$$\overline{\Delta p}(x_{\mathrm{D}},y_{\mathrm{D}},z_{\mathrm{D}},s)=\frac{1.842\times10^{-3}\sqrt{3.6}\mu}{2L\sqrt{k_{\mathrm{h}}k_{\mathrm{v}}}}\overline{q}(s)(\Delta-\Delta')\tag{A.13}$$

where

$$\begin{aligned}\Delta&=2\sum_{n=-\infty}^{n=+\infty}\frac{\exp\left[-\sqrt{s}\sqrt{3.6}\sqrt{(x_{\mathrm{D}}-x_{\mathrm{wD}})^2+(y_{\mathrm{D}}-y_{\mathrm{wD}})^2+(z_{\mathrm{D}}-z_{\mathrm{wD}}-2\cdot2nh_{\mathrm{D}})^2}\right]}{\sqrt{3.6}\sqrt{(x_{\mathrm{D}}-x_{\mathrm{wD}})^2+(y_{\mathrm{D}}-y_{\mathrm{wD}})^2+(z_{\mathrm{D}}-z_{\mathrm{wD}}-2\cdot2nh_{\mathrm{D}})^2}}\\&-\sum_{n=-\infty}^{n=+\infty}\frac{\exp\left[-\sqrt{s}\sqrt{3.6}\sqrt{(x_{\mathrm{D}}-x_{\mathrm{wD}})^2+(y_{\mathrm{D}}-y_{\mathrm{wD}})^2+(z_{\mathrm{D}}-z_{\mathrm{wD}}-2nh_{\mathrm{D}})^2}\right]}{\sqrt{3.6}\sqrt{(x_{\mathrm{D}}-x_{\mathrm{wD}})^2+(y_{\mathrm{D}}-y_{\mathrm{wD}})^2+(z_{\mathrm{D}}-z_{\mathrm{wD}}-2nh_{\mathrm{D}})^2}}\\\Delta'&=2\sum_{n=-\infty}^{n=+\infty}\frac{\exp\left[-\sqrt{s}\sqrt{3.6}\sqrt{(x_{\mathrm{D}}-x_{\mathrm{wD}})^2+(y_{\mathrm{D}}-y_{\mathrm{wD}})^2+(z_{\mathrm{D}}+z_{\mathrm{wD}}-2\cdot2nh_{\mathrm{D}})^2}\right]}{\sqrt{3.6}\sqrt{(x_{\mathrm{D}}-x_{\mathrm{wD}})^2+(y_{\mathrm{D}}-y_{\mathrm{wD}})^2+(z_{\mathrm{D}}+z_{\mathrm{wD}}-2\cdot2nh_{\mathrm{D}})^2}}\\&-\sum_{n=-\infty}^{n=+\infty}\frac{\exp\left[-\sqrt{s}\sqrt{3.6}\sqrt{(x_{\mathrm{D}}-x_{\mathrm{wD}})^2+(y_{\mathrm{D}}-y_{\mathrm{wD}})^2+(z_{\mathrm{D}}+z_{\mathrm{wD}}-2nh_{\mathrm{D}})^2}\right]}{\sqrt{3.6}\sqrt{(x_{\mathrm{D}}-x_{\mathrm{wD}})^2+(y_{\mathrm{D}}-y_{\mathrm{wD}})^2+(z_{\mathrm{D}}+z_{\mathrm{wD}}-2nh_{\mathrm{D}})^2}}\end{aligned}\tag{A.14}$$

Using the Poisson summation formula and the integral expression of the second modified Bessel function:

$$\sum_{n=-\infty}^{+\infty}\exp\left[-\frac{(m-2nr)^2}{4t}\right]=\frac{\sqrt{\pi t}}{r}\left[1+2\sum_{n=1}^{+\infty}\exp\left(-\frac{n^2\pi^2 t}{r^2}\right)\cos\left(n\pi\frac{m}{r}\right)\right] \tag{A.15}$$

$$\begin{aligned}&\sum_{n=-\infty}^{+\infty}\frac{\exp\left(-\sqrt{3.6}\sqrt{R_{xy,\mathrm{D}}^2+(z_\mathrm{D}-z_{\mathrm{wD}}-2nh_\mathrm{D})^2}\cdot\sqrt{s}\right)}{\sqrt{3.6}\sqrt{R_{xy,\mathrm{D}}^2+(z_\mathrm{D}-z_{\mathrm{wD}}-2nh_\mathrm{D})^2}}\\&=\frac{1}{\sqrt{3.6}h_\mathrm{D}}\left[K_0\left(\sqrt{3.6}R_{xy,\mathrm{D}}\sqrt{s}\right)+2\sum_{n=1}^{+\infty}K_0\left(\sqrt{3.6}R_{xy,\mathrm{D}}\sqrt{s+\frac{n^2\pi^2}{3.6h_\mathrm{D}^2}}\right)\cos\left(n\pi\frac{z_\mathrm{D}-z_{\mathrm{wD}}}{h_\mathrm{D}}\right)\right]\end{aligned} \tag{A.16}$$

$$\begin{aligned}&\sum_{n=-\infty}^{+\infty}\frac{\exp\left(-\sqrt{3.6}\sqrt{R_{xy,\mathrm{D}}^2+(z_\mathrm{D}+z_{\mathrm{wD}}-2nh_\mathrm{D})^2}\cdot\sqrt{s}\right)}{\sqrt{3.6}\sqrt{R_{xy,\mathrm{D}}^2+(z_\mathrm{D}+z_{\mathrm{wD}}-2nh_\mathrm{D})^2}}\\&=\frac{1}{\sqrt{3.6}h_\mathrm{D}}\left[K_0\left(\sqrt{3.6}R_{xy,\mathrm{D}}\sqrt{s}\right)+2\sum_{n=1}^{+\infty}K_0\left(\sqrt{3.6}R_{xy,\mathrm{D}}\sqrt{s+\frac{n^2\pi^2}{3.6h_\mathrm{D}^2}}\right)\cos\left(n\pi\frac{z_\mathrm{D}+z_{\mathrm{wD}}}{h_\mathrm{D}}\right)\right]\end{aligned} \tag{A.17}$$

$$\begin{aligned}&2\sum_{n=-\infty}^{+\infty}\frac{\exp\left(-\sqrt{3.6}\sqrt{R_{xy,\mathrm{D}}^2+(z_\mathrm{D}-z_{\mathrm{wD}}-2\cdot2nh_\mathrm{D})^2}\cdot\sqrt{s}\right)}{\sqrt{3.6}\sqrt{R_{xy,\mathrm{D}}^2+(z_\mathrm{D}-z_{\mathrm{wD}}-2\cdot2nh_\mathrm{D})^2}}\\&=\frac{1}{\sqrt{3.6}h_\mathrm{D}}\left[K_0\left(\sqrt{3.6}R_{xy,\mathrm{D}}\sqrt{s}\right)+2\sum_{n=1}^{+\infty}K_0\left(\sqrt{3.6}R_{xy,\mathrm{D}}\sqrt{s+\frac{n^2\pi^2}{3.6\times4h_\mathrm{D}^2}}\right)\cos\left(n\pi\frac{z_\mathrm{D}-z_{\mathrm{wD}}}{2h_\mathrm{D}}\right)\right]\end{aligned} \tag{A.18}$$

$$\begin{aligned}&2\sum_{n=-\infty}^{+\infty}\frac{\exp\left(-\sqrt{3.6}\sqrt{R_{xy,\mathrm{D}}^2+(z_\mathrm{D}-z_{\mathrm{wD}}-2\cdot2nh_\mathrm{D})^2}\cdot\sqrt{s}\right)}{\sqrt{3.6}\sqrt{R_{xy,\mathrm{D}}^2+(z_\mathrm{D}-z_{\mathrm{wD}}-2\cdot2nh_\mathrm{D})^2}}\\&=\frac{1}{\sqrt{3.6}h_\mathrm{D}}\left[K_0\left(\sqrt{3.6}R_{xy,\mathrm{D}}\sqrt{s}\right)+2\sum_{n=1}^{+\infty}K_0\left(\sqrt{3.6}R_{xy,\mathrm{D}}\sqrt{s+\frac{n^2\pi^2}{3.6\times4h_\mathrm{D}^2}}\right)\cos\left(n\pi\frac{z_\mathrm{D}+z_{\mathrm{wD}}}{2h_\mathrm{D}}\right)\right]\end{aligned} \tag{A.19}$$

where $R_{xy,\mathrm{D}}^2=(x_\mathrm{D}-x_{\mathrm{wD}})^2+(y_\mathrm{D}-y_{\mathrm{wD}})^2$.

Taking account of the interference between perforations, the pressure distribution of the main wellbore of the herringbone well at the point $M(x_\mathrm{w}, y_\mathrm{w}, z_\mathrm{w})$ in the reservoir is obtained as Eq. (20) according to the pressure drop superposition principle:

$$\overline{\Delta p}(x_\mathrm{D},y_\mathrm{D},z_\mathrm{D},s)=\frac{1.842\times10^{-3}\mu}{2L\sqrt{k_\mathrm{v}k_\mathrm{h}}}\overline{q}(s)\frac{2}{h_\mathrm{D}}\left\{\sum_{n=1}^{+\infty}K_0\left[\sqrt{3.6}R_{xy,\mathrm{D}}\sqrt{s+\frac{(2n-1)^2\pi^2}{3.6\times4h_\mathrm{D}^2}}\right]\sin\frac{(2n-1)\pi z_\mathrm{D}}{2h_\mathrm{D}}\sin\frac{(2n-1)\pi z_{\mathrm{wD}}}{2h_\mathrm{D}}\right\} \tag{A.20}$$

References

Bahadori, A., Nouri, A., 2012. Prediction of critical oil rate for bottom water coning in anisotropic and homogeneous formations. J. Petrol. Sci. Eng. 82, 125–129. https://doi.org/10.1016/j.petrol.2012.01.016.

Bazitov, M.V., Golovko, I.S., Konosov, D.A., et al., 2015. First fishbone well drilling at Vankorskoe field. In: SPE Russian Petroleum Technology Conference. https://doi.org/10.2118/176510-MS.

Bournazel, C., Jeanson, B., 1971. Fast water-coning evaluation method. In: Fall Meeting of the Society of Petroleum Engineers of AIME. Society of Petroleum Engineers.

Bruining, J., VanDuijn, C., Schotting, R., 1991. Simulation of coning in bottom water driven reservoirs. Trans. Porous Media 6 (1), 35–69. https://doi.org/10.1007/BF00136821.

Cai, J., Qin, X., Xia, X., et al., 2024. Numerical modeling of multiphase flow in porous media considering micro- and nanoscale effects: A comprehensive review. Gas Sci. Eng. 131, 205441. https://doi.org/10.1016/J.JGSCE.2024.205441.

Cai, J., Qin, X., Wang, H., et al., 2025. Pore-scale investigation of forced imbibition in porous rocks through interface curvature and pore topology analysis. J. Rock Mech. Geotech. Eng. 17 (1), 245–257. https://doi.org/10.1016/J.JRMGE.2024.02.047.

Fan, Y., Han, G., Yang, C., 2006. Production forecast for herringbone well and optimum configuration of lateral holes. Acta Pretrolei Sinica. 27 (4), 101–104 (in Chinese).

Filho, J., Jose, S., Sepehrnoori, K., et al., 2015. Modeling fishbones using the embedded discrete fracture model formulation: Sensitivity analysis and history matching. In: SPE Annual Technical Conference and Exhibition. https://doi.org/10.2118/175124-MS.

Fuad, H., Qasem, I., 2024. Simulation and performance prediction of partially naturally fractured reservoirs under solution gas drive primary recovery and gas injection processes. J. Pet. Explor. Prod. Technol. 14 (5), 1259–1282. https://doi.org/10.1007/S13202-024-01764-0.

Gang, R., Gao, H., Li, B., et al., 2024. A new productivity prediction model for multi-fractured horizontal wells in tight oil reservoirs. J. Phys. Conf. 2834 (1), 012191. https://doi.org/10.1088/1742-6596/2834/1/012191.

Haugen, S.A., Lund, O., Hoyland, L.A., 1988. Statfjord Field: Development strategy and reservoir management. J. Pet. Technol. 40 (7), 863–873. https://doi.org/10.2118/16961-PA.

Luo, W., Zhou, Y., Wang, X., 2008. A novel 3-D model for the water cresting in horizontal wells. J. Hydrodyn. 20 (6), 749–755. https://doi.org/10.1016/S1001-6058(09)60011-1.

Luo, P., Meng, J., Li, H., et al., 2017. Successful field trials of water control in high water cut wells using an improved down hole water sink/drainage system. In: Abu Dhabi International Petroleum Exhibition & Conference. https://doi.org/10.2118/188958-MS.

Lux, M., Szanyi, J., Toth, T., 2016. Evaluation and optimization of multi-lateral wells using MODFLOW unstructured grids. Open Geosci. 8, 39–44. https://doi.org/10.1515/geo-2016-0004.

McCarthy, J., 1994. Analytical solutions of 2D cresting models using the hodograph method. Trans. Porous Media 15 (3), 251–269. https://doi.org/10.1007/BF00613281.

Muskat, M., Wyckoff, R.D., 1935. An approximate theory of water coning in oil production. Petrol. Trans. AIME 114, 144–163. https://doi.org/10.2118/14210-MS.

Ouyang, L., Aziz, K., 2001. A general single-phase wellbore/reservoir coupling model for multilateral wells. SPE Reservoir Eval. Eng. 4, 327–335. https://doi.org/10.2118/72467-PA.

Ozkan, E., Raghavan, R., 1989. Performance of horizontal wells subject to bottom water drive. SPE Reserv. Eng. 5, 375–383. https://doi.org/10.2118/18559-PA.

Ozkan, E., Raghavan, R., 1990. A breakthrough time correlation for coning toward horizontal wells. In: European Petroleum Conference. https://doi.org/10.2118/20964-MS.

Permadi, P., Jayadi, T., 2010. An improved water coning calculation for horizontal wells. In: SPE Russian Oil and Gas Conference and Exhibition,. https://doi.org/10.2118/133162-MS.

Permadi, P., Lee, R., Kartoatmodjo, R., 1995. Behavior of water cresting under horizontal wells. In: SPE Annual Technical Conference and Exhibition. https://doi.org/10.2118/30743-MS.

Qiu, K., Fan, K., Chen, X., et al., 2023. A new approach for production prediction in onshore and offshore tight oil reservoir. J. Mar. Sci. Eng. 11 (11). https://doi.org/10.3390/JMSE11112079.

Shi, K., Chen, J., Pang, X., et al., 2023. Wettability of different clay mineral surfaces in shale: implications from molecular dynamics simulations. Pet. Sci. 20 (2), 689–704. https://doi.org/10.1016/J.PETSCI.2023.02.001.

Shi, K., Chen, J., Pang, X., et al., 2024. Average molecular structure model of shale kerogen: experimental characterization, structural reconstruction, and pyrolysis analysis. Fuel 355, 129474. https://doi.org/10.1016/j.fuel.2023.129474.

Song, X., Zhang, C., Shi, Y., et al., 2019. Production performance of oil shale in-situ conversion with multilateral wells. Energy 189, 116145. https://doi.org/10.1016/j.energy.2019.116145.

Tabatabaei, M., Ghalambor, A., Guo, B., 2012. An analytical solution for water coning in vertical wells. SPE Prod. Oper. 27 (2), 195–204. https://doi.org/10.2118/113106-PA.

Tong, S., Wang, F., Gao, H., et al., 2024. A machine learning-based method for analyzing factors influencing production capacity and production forecasting in fractured tight oil reservoirs. Int. J. Hydrogen Energy 70, 136–145. https://doi.org/10.1016/J.IJHYDENE.2024.05.036.

Wang, H., Guo, J., Zhang, L., 2017. A semi-analytical model for multilateral horizontal wells in low-permeability naturally fractured reservoirs. J. Petrol. Sci. Eng. 149, 564–578. https://doi.org/10.1016/j.petrol.2016.11.002.

Wang, L., Zhang, Y., Zou, R., et al., 2025a. Dynamics of oil–CO_2–water three-phase under the nanopore confinement effect: implications for CO_2 enhanced shale oil recovery and carbon storage. Separ. Purif. Technol. 354, 128892. https://doi.org/10.1016/J.SEPPUR.2024.128892.

Wang, Y., Guo, W., Sun, G., et al., 2025b. Remaining oil distribution and enhanced oil recovery mechanisms through multi-well water and gas injection in weathered crust reservoirs. Processes 13 (1), 241. https://doi.org/10.3390/PR13010241.

Wang, Z., Fu, X., Guo, P., et al., 2015. Gas-liquid flowing process in a horizontal well with premature liquid loading. J. Nat. Gas Sci. Eng. 25 (7), 207–214. https://doi.org/10.1016/j.jngse.2015.05.003.

Yi, X., Tang, J., 2023. Optimization of process parameters for acid fracturing assisted herringbone well SAGD. Vibroeng. Proc. 49227–49232. https://doi.org/10.21595/VP.2023.23237.

Yu, F., Huang, G., Ni, H., et al., 2019. Analysis of the main factors affecting bottom hole assembly Re-entry into main hole in forward drilling of fishbone wells. J. Petrol. Sci. Eng. 189, 107018. https://doi.org/10.1016/j.petrol.2020.107018.

Yue, P., Chen, X., Liu, H., et al., 2015. The critical parameters of a horizontal well influenced by a semi-permeable barrier considering thickness in a bottom water reservoir. J. Petrol. Sci. Eng. 129, 88–96. https://doi.org/10.1016/j.petrol.2015.02.029.

Yue, P., Jia, B., Sheng, J., et al., 2019. A coupling model of water breakthrough time for a multilateral horizontal well in a bottom water-drive reservoir. J. Petrol. Sci. Eng. 177, 317–330. https://doi.org/10.1016/j.petrol.2019.02.033.

Yue, P., Guo, C., Cheng, X., et al., 2020. A transient flow model for multilateral horizontal wells in bottom water drive reservoirs. Int. J. Oil Gas Coal Technol. 24 (1), 1–17. https://doi.org/10.1504/IJOGCT.2019.10022587.

Yue, P., Zhou, J., Kang, L., et al., 2021. Reservoir and wellbore flow coupling model for fishbone multilateral wells in bottom water drive reservoirs. J. Energy Resour. Technol. 143, 123001. https://doi.org/10.1115/1.4050053.

Zhai, L., Yang, M., Yan, C., et al., 2022. Dynamic distribution characteristics of oil and water during water flooding in a fishbone well with different branch angles. ACS Omega 7 (31), 27206–27215. https://doi.org/10.1021/ACSOMEGA.2C01918.

Zhang, L., Gu, D., 2024. New model for predicting production capacity of horizontal well volume fracturing in tight reservoirs. ACS Omega 9 (10), 11806–11819. https://doi.org/10.1021/ACSOMEGA.3C09051.

Zhang, K., Jin, Z., Li, G., et al., 2023. Gas adsorptions of geological carbon storage with enhanced gas recovery. Separ. Purif. Technol. 311, 123260. https://doi.org/10.1016/j.seppur.2023.123260.

Zhou, X., Zeng, F., Zhang, L., 2016. Improving steam-assisted gravity drainage performance in oil sands with a top water zone using polymer injection and the fishbone well pattern. Fuel 184, 449–465. https://doi.org/10.1016/j.fuel.2016.07.040.

Zhou, Z., Cui, C., Zheng, D., et al., 2023. Transient productivity analysis and completion parameter optimization of perforating herringbone wells. ACS Omega 8 (20), 17841–17855. https://doi.org/10.1021/ACSOMEGA.3C00819.